ENERGY RECONSTRUCTION ALGORITHMS AND THEIR INFLUENCE ON THE ATLAS TILE CALORIMETER *

E. FULLANA†
IFIC - Instituto de Física Corpuscular
Edificio Institutos de Investigación,
Polígono la coma s/n, Paterna (Valencia-SPAIN)
E-mail: Esteban.Fullana.Torregrosa@cern.ch

This paper describes the technique of energy reconstruction with different algorithms when applied to calorimeter data from collider experiments. Two algorithms are explained: Flat Filtering (FF) and Optimal Filtering (OF). Their impact on calorimeter energy resolution and linearity is studied using real data from the ATLAS Tile Calorimeter testbeam program.

1. Introduction

Energy reconstruction algorithms in colliders are designed to reconstruct the energy deposited in a read out cell of calorimeters from the digital samples of the analog signal.

The energy reconstruction algorithms studied in this paper will be implemented in the Read Out Driver (ROD) cards which are part of the ATLAS DAQ electronics. The ROD, a 9U VME electronic card, reads the optical fibers from the front-end electronics [1]. The fibers transmit all the information of an event selected by the first level trigger in digital format. The ROD motherboard is designed to hold mezzanine cards which are equipped with last generation Digital Signal Processors (DSP). The DSP can be programmed to implement the energy reconstruction algorithms. Once the energy is calculated the information is sent to the second level trigger, the next step of the data acquisition chain. The maximum allowed rate of the first level trigger ($\sim$ 100 kHz) and the computing power limitations of the DSPs impose severe constraints to the complexity of the algorithms. However good performance of second level trigger requires high accuracy of the

*This work is supported by Ministerio de Ciencia y Tecnologia of Spain
†From Tile subsystem of ATLAS collaboration

energy reconstruction. Therefore the algorithm should reach a compromise between both magnitudes. The two algorithms described here fulfill the non-complexity requirement. Their energy reconstruction accuracy will be studied with real data in the present paper.

2. Flat filtering algorithm

The Flat Filtering algorithm (FF) calculates energy as the sum of part or all the samples in a single event. The simplest way to implement the algorithm is to sum all the samples as:

$$E = \sum_{i=1}^{N} (S_i - Ped) \tag{1}$$

where E is the energy in ADC counts, S_i are the digital samples, N is the number of samples and Ped is the pedestal.

When the sampling time (sampling period times the number of samples) is greater than the signal duration the number of samples in the sum should be reduced in order to minimize noise and improve the resolution. In the present paper the FF algorithm was implemented as the sum of all the samples. Although the number of noise samples is not zero in the Tilecal testbeam environment, they do not degrade the resolution significantly. Moreover this implementation is simpler and it allows a consistent comparison with the Optimal Filtering (OF) algorithm making the number of input samples equal in both algorithms.

3. Optimal filtering algorithm

The implementation of OF algorithms in liquid ionization calorimeters working in a high luminosity environment was first proposed in 1994[2]. This type of calorimeters have a long time signal, several times greater than the time between bunch crossings. The signal must be shortened in order to reduce the amount of minimum bias noise. However a very short timing decreases the signal to electronic noise ratio. The compromise between these two factors defines a time which optimizes the minimization of both noise sources. This optimized time is hardware fixed in the shaper. However a permanent time optimization is not possible due to minimum bias noise dependence on luminosity. OF is designed to minimize noise even if the shaper time is not at the optimized value.

The scenario for the ATLAS Tile Calorimeter (Tilecal) is different. The read out is based on photomultipliers whose short signal ($\sim$ 20 ns) avoids

the problem of optimization. However the signal has also contributions from pile up and electronic noise, therefore this algorithm could be useful in this type of calorimeter.

The reconstructed energy, in this algorithm, equals to a weighted sum of the samples:

$$E = \sum_{i=1}^{N} a_i(S_i - Ped) \tag{2}$$

where a_i are the OF weights. Apart from the energy reconstruction, OF also provides other quantities like time phase reconstruction by changing a_i by another set of weights.

The OF weights are calculated from special calibration events and applied online event by event. The calculation of weights requires information about the noise and the signal shape form at the input of the digitizer. The OF weights are the solution (for 5 input samples) of the following equation:

$$\begin{pmatrix} R_{11} & R_{12} & R_{13} & R_{14} & R_{15} & g_1 & g'_1 \\ R_{21} & R_{22} & R_{23} & R_{24} & R_{25} & g_2 & g'_2 \\ R_{31} & R_{32} & R_{33} & R_{34} & R_{35} & g_3 & g'_3 \\ R_{41} & R_{42} & R_{43} & R_{44} & R_{45} & g_4 & g'_4 \\ R_{51} & R_{52} & R_{53} & R_{54} & R_{55} & g_5 & g'_5 \\ g_1 & g_2 & g_3 & g_4 & g_5 & 0 & 0 \\ g'_1 & g'_2 & g'_3 & g'_4 & g'_5 & 0 & 0 \end{pmatrix} \cdot \begin{pmatrix} a_1 \\ a_2 \\ a_3 \\ a_4 \\ a_5 \\ \gamma \\ \kappa \end{pmatrix} = \begin{pmatrix} 0 \\ 0 \\ 0 \\ 0 \\ 0 \\ 1 \\ 0 \end{pmatrix} \tag{3}$$

where R_{ij} represents the noise autocorrelation matrix elements. The g_i are the normalized shape form factors calculated from the normalized shape form function (Fig. 1 left). The g_3 term sets the reference of the time reconstruction while the others are spaced from this reference time the corresponding sampling periods. The g'_i terms are calculated from the derivative of the normalized shape form function and at the same times as g_i.

In the present analysis the noise autocorrelation matrix is made equal to the unitary matrix because the correlation of noise samples was not significant. This small correlation was detected in all data acquisition periods. In any case, the impact of R_{ij} on the resolution was studied in the past and the conclusion was that R_{ij} does not change the resolution significantly in the Tilecal testbeam environment[3]. This situation could change in the LHC where minimum bias noise will be present. The procedure to calculate the

noise autocorrelation matrix in the future is still an open question which will be decided according to results on LHC data.

The shape form is reconstructed from calibration events. The Tilecal front-end electronics includes a calibration system based on the discharge of a capacitor. The system simulates as close as possible the current signal of the photomultiplier. The time between the discharge and the digitizer can be set at different values (phases) covering the sampling period in steps of ~ 0.7 ns. A proper combination of the samples from all the phases reconstructs the shape form. Finally the g_i and g_i' factors are calculated from the analytical function fitted to the shape form. This approach assumes that the shape form of the calibration system and the output shape form of the photomultiplier are equal. However there is a difference between both shape forms of about 10% in area. In the future a new method of shape form reconstruction must be developed in order to avoid this systematic error.

OF weights are calculated for a certain time phase between the event production and the digitizer clock. This phase should be fixed event by event for a proper OF performance. This is not a problem in a collider environment when the events are synchronous. However this is not the situation at the Tilecal testbeam. The testbeam is asynchronous and OF would not work properly. However the problem was solved by using the time reconstruction and introducing iterations in the algorithm. A convergence criteria was set in the time reconstruction to be lower than a 5% of the digitizer period. At the same time this algorithm monitors the quality of the reconstruction (χ) by applying:

$$\chi E = \sum_{i=1}^{N} ABS((S_i - Ped) - Eg_i) \tag{4}$$

This functionality double checks the efficiency of the iteration process.

4. Results

4.1. *Data acquisition*

The Tilecal detector is an iron-scintillator non-compensating sampling calorimeter. The detector has a cylindrical shape divided in 64 modules each covering 5.6^0 in azimuth. The scintillator tiles are placed in planes perpendicular to the beam direction and are read out by two WLS (wavelenght shifter) fibers (see Fig. 1 right). A group of fibers defines a cell which

is read out by two photomultipliers. This configuration allows a very good hermeticity[4].

Part of the 256 Tilecal modules are calibrated at dedicated testbeam setups. The SPS accelerator facility at CERN provides a single beam of electrons, pions or muons with an energy range from 350 GeV to 1 GeV. The Tilecal detector modules are placed in a movable table which allow the modules to be calibrated under several beam directions.

4.2. *Energy resolution*

The energy deposited in a calorimeter module by pions and electrons is reconstructed in order to study the performance of FF and OF algorithms. The energy is computed as the sum of the energy deposited in all the cells in one module of the calorimeter. In the case of pion reconstruction the whole shower is not fully contained within the module degrading the resolution. In the case of electron reconstruction the shower is almost fully contained within a single cell of the module, however the other cells of the module, which only contain noise, degrade the resolution. Therefore, the resolutions given in this paper are not optimized but they are obtained under the same conditions in both algorithms which is the important point to make a consistent comparison between them.

The resolutions for pion reconstruction are summarized in Table 1 and shown in Fig. 2 left as a function of energy and for a pseudorapidity of 0.35. The resolutions are similar at high energies and the improvement in OF becomes only important as the energy decreases. The reason is the energy resolution loss by the noise effect which is more important as the signal to noise ratio decreases. The same conclusion can be applied to the electron case shown in Table 2 for the case of 90^0 incident angles. Table 3 shows the sampling, noise and constant term of the standard energy resolution parametrization for electrons and pions. The fit proves that the OF noise term is lower than the FF one in both cases.

4.3. *Linearity*

The energy reconstruction algorithms provide the energy in ADC counts. This magnitude is converted to charge released by the photomultiplier, in pC, by proper applying calibration constants. These constants are calculated from data taken with charge injection runs. In order to study the linearity of FF and OF algorithms Fig. 3 shows the pC response divided by the energy of the beam.

The Figures show the algorithms effect on linearity. The response to electrons is higher than the response to pions by a factor of ~ 1.3 in both algorithms. The result is expected because this factor does not depend on the algorithm but on the ratio of the amount of active and passive material. The response of FF is $\sim 10\%$ greater at high energies than the response of OF because the shape form of charge injection is $\sim 10\%$ greater in area than the shape form of physics. As FF is an area based algorithm, this difference is translated to the energy reconstruction by the same amount. This $\sim 10\%$ difference is present only at high energies, at lower energies there is not variation on the response between the algorithms. This result could be interpreted as a sign of the dependence of the area difference between both shape forms with the energy.

5. Conclusions

The improvement in the low energy resolution of OF with respect to FF has been proved. The data was obtained from the Tilecal testbeam facility in a Tilecal module impinged by the SPS calibration beam. The OF algorithm is designed to minimize minimum bias and electronic noise. Its effect in Tilecal testbeam environment where there is not minimum bias is remarkable in the region where the signal to noise ratio is low, i.e. where the electronic noise is not negligible.

The linearity performance has also been shown. There is not linearity loss by using OF instead of FF. There are signs of less sensitivity to the shape form variations of OF with respect to FF although this should be double checked.

Acknowledgments

I would like to thank Rupert Leitner, Robert Stanek, Richard Teuscher and Tomas Davidek for the endless discussions about Tilecal energy resolution and response. At the same time I would like to mention Bill Cleland, without his help and expertise this paper would not have been possible. Of course I am very grateful to Emilio Higon, Juan Valls and the people of Tilecal Valencia group for the detailed scrutiny, interest, patient, suggestions, advices, good ideas...

References

1. J. Castelo, E.Fullana, J. Torres, *Proceedings of the LECC 2002 8th Workshop on Electronics for LHC Experiment.* **CERN-LHCC-2002-03**

2. W.E. Cleland, E.G. Stern, *Nucl. Instr. and Meth. in Phys. Res. A* **338**, 467-497 (1994).
3. F. Camarena, J. Castelo, E. Fullana, *ATLAS internal note.* **ATL-TILECAL-2002-015** (2002).
4. ATLAS/Tile Calorimeter Collaboration, *Technical Design Report.* **CERN/LHCC 96-42** (1996).

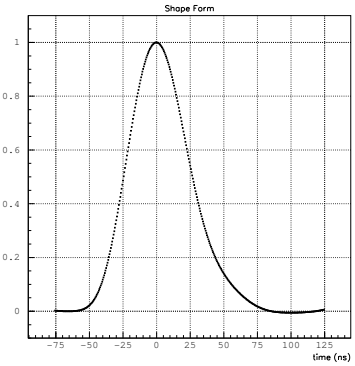

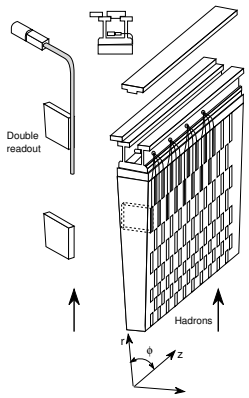

Figure 1. Left: Photomultiplier shape form at the input of the digitizer. Right: Tilecal module layout.

Table 1. Resolution of pions impinging the detector with pseudo-rapidity 0.35

	350 GeV	180 GeV	100 GeV	20 GeV	9 GeV	5 GeV
OF	7.6%	8.4%	10.5 %	16.4%	26.5%	36.9%
FF	7.8%	8.4%	10.8 %	16.6%	28.1%	40.8%

Table 2. Resolution of electrons with an incident angle of 90^0, i.e. perpendicular to the scintillator plane

	180 GeV	100 GeV	50 GeV	20 GeV	9 GeV	2 GeV
OF	2.2%	3.1%	4.0 %	6.0%	8.1%	18.7%
FF	2.3%	3.4%	4.8 %	6.1%	8.7%	21.6%

Table 3. Sampling (a), noise (b) and constant (c) term of energy resolution for pions and electrons obtained from the fit of data to the parametrization: $\frac{\sigma}{E} = \frac{a}{\sqrt{E}} \otimes \frac{b}{E} \otimes c$

	Pions			Electrons		
	a	b	c	a	b	c
OF	0.66	1.07	0.07	0.26	.007	.002
FF	0.64	1.43	0.07	0.23	.271	.028

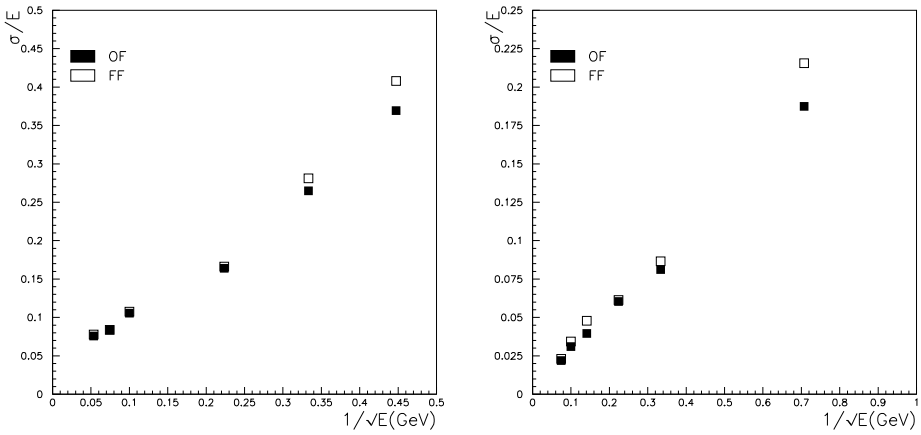

Figure 2. Energy resolution: left, pions with incident angle .35 eta projective. Right, electrons with incident angle perpendicular to the scintillator plane

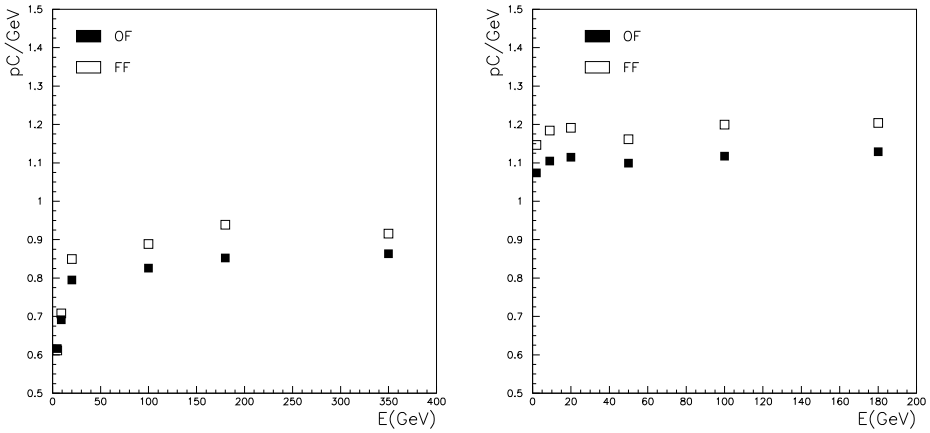

Figure 3. Linearity: pC divided by the energy of the beam; left pions, right electrons